Theor Chem Account (2008) 119:81–97
DOI 10.1007/s00214-006-0183-4

REGULAR ARTICLE

Tight β-turns in peptides. DFT-based study of infrared absorption and vibrational circular dichroism for various conformers including solvent effects

Joohyun Kim · Josef Kapitán · Ahmed Lakhani · Petr Bouř · Timothy A. Keiderling

Received: 5 August 2006 / Accepted: 5 November 2006 / Published online: 22 December 2006

Abstract Vibrational circular dichroism (VCD) has had a large impact on configurational studies of organic molecules largely due to the theoretical advances made by Philip Stephens and co-workers. For peptides, the structural issue is not one of the configuration, but of conformation, and the flexibility of the oligomeric structure raises major computational challenges. Turns are a vital aspect of peptide and protein conformation that allow such structures to fold into a compact unit. However, unlike helices and sheets, they are not extended repeating structures, but each residue has a different local conformation. Also, when turns are part of larger peptides their termini are connected to completely different structural elements. We have done extended comparative density functional theory (DFT) computations to characterize the expected spectral contributions of selected turn structures to the amide IR and VCD spectra of peptides. The isolated vacuum results for tri-amide turns (Ac-X-Y-NH_2) of a few different sequences are compared with calculations involving correction for solvation effects. In particular, we looked at the sequence variation in spectra and structure between Ala-Ala, Aib-Gly and D-Pro-Gly for the turn-specific X–Y residues. The nature of some turn-associated, amide originating, spectral transitions are developed and tested.

J. Kim · J. Kapitán · A. Lakhani · T. A. Keiderling (✉)
Department of Chemistry, University of Illinois at Chicago, 845 W. Taylor St. (m/c 111), Chicago, IL 60607-7061, USA
e-mail: tak@uic.edu

P. Bouř
Institute of Organic Chemistry and Biochemistry, Czech Academy of Sciences, Flemingovo nám. 2, Prague 6, 16610, Czech Republic

Keywords Peptide beta-turn · Density functional theory (DFT) · Infrared (IR) absorption · Vibrational circular dichroism (VCD) · Solvation

Introduction

The past decades have seen a large growth in the use of vibrational spectroscopic techniques to determine secondary structure in proteins and peptides [1–8]. Although IR has long been an important tool of peptide and protein chemists, the development and wide availability of Fourier transform IR (FTIR) instruments with exceptional signal-to-noise ratio has stimulated its use for addressing structural questions. Adding polarization sensitivity, through chirally sensitive vibrational circular dichroism (VCD) measurements, using methods that were originally developed in the laboratories of Philip Stephens [9] has added discrimination to these vibrational analyses [6–8,10]. Similarly, continued advances in Raman spectroscopy, including resonance Raman effects and Raman optical activity, have had similar impact [11–14]. The development of modern quantum chemical techniques to simulate IR and VCD spectra, such as those developed and refined by Stephens and co-workers in the last two decades [15–19], has moved analyses of such vibrational spectra from the realm of totally empirical to highly theoretical. We and others have attempted to apply those computational methods to the simulation of IR and VCD spectra for peptides in an effort to determine conformation. In this paper we will present some specific theoretical models of the spectra of selected, non-zwitterionic β-turns which mimic segments of hairpins and proteins and may prove useful for future studies of peptide conformation. We

have made no attempt at this point to review the continually growing field of small peptide conformational determination.

Peptides and proteins (apart from unordered segments) have two dominant types of extended secondary structure, α-helices and β-sheets, where strands develop repeating ϕ, ψ torsional angles. The most common structural unit in globular proteins is the α-helix, characterized by a quite regular $i \rightarrow i+4$ H-bonding, 3.6 residues per turn and main chain torsional angles of approximately $\phi = -57°$, $\psi = -47°$. The regularity of this structure, with its H-bonds (and C=O groups) oriented almost parallel to the helix axis, has enhanced efforts to simulate its spectra and extensive successful theoretical studies of α-helical structure and spectra have appeared [20–28]. Other helical geometries are stabilized by H-bonds, of which the 3_{10}-helix has $i \rightarrow i+3$ H-bonds, also along the axis, and often is found in shorter helical segments or at the C-terminal of proteins [29,30]. This conformation is sometimes termed a repeating type III β-turn, but the angles of the cross-linked H-bond could be different. Differentiation of 3_{10}-helices and α-helices, not easily done with IR or CD, is considered to be a major success of VCD in peptide conformational analyses, enabled by the comparison of multiple resolved bands [29,31–35]. For short peptides, the 3_{10}-helix is the more stable structure in general, and in our calculational tests using quantum mechanical (QM) methods for geometry optimization, which included spectral simulations, the α-helix form was converted to 3_{10} helix for short peptides in vacuum but was more stable for long sequences and in solution [36]. Other groups have also theoretically modeled the 3_{10}-helical stability problem and obtained consistent results using different methods [37,38].

Another helical conformation gaining much recent attention is the left-handed 3_1-helix (formally a 3_2-helix), 3-residues per turn, with *trans* amide C=O groups pointing out, perpendicular to the helical axis. This is often termed the PPII conformation due to its being the stable form for poly-L-proline II (water soluble). Because of its contribution to a wide range of unfolded protein and peptide structures, the 3_1-helix is thought to be a major component of what was historically termed a "random coil" [39–43]. This helix is significantly different in that the strands are essentially extended and the C=O groups are oriented out into solution, which can explain terming it an "extended helix" in the original assignment of this underlying "random coil" structure by Sam Krimm and colleagues [44–46]. Such a conformation is well suited to stabilize an unfolded peptide by providing solvent access and thus energetically favorable H-bond formation for the amide function in water.

The second most common structure is the β-sheet, which involves relatively extended strands that are characterized by cross-strand (hydrogen) H-bonding. This would ideally form a 2_1-helix, with two residues per turn and the C=O groups alternately pointing in opposite directions. The relationship of a sheet conformation with the 3_1-helix is essentially due to the relative degree of strand twist, 180° versus 120°. In fact most sheets are not flat, but are twisted with an overall right handed sense, which means the strands are locally left handed (one C=O to the next C=O in sequence) with what might be viewed as a helical conformation having a bit more than two residues per turn [47–49].

To form the sheet in a molecule composed of a single strand (such as is common in a protein) the local peptide conformation must change to encompass a loop or in many cases a tight turn with a $i \rightarrow i+3$ H-bond from C=O (i) to N-H ($i+3$). The $i+1$ and $i+2$ C=O groups are thus oriented out into the solvent, but have varying degrees of shielding depending on the turn conformation and side-chains. There are a large number of possible turn geometries [50–54] which can fit this constraint, but this conformational variety also makes spectral characterization of a turn difficult.

Turns, whose local, internal ϕ, ψ characteristics can reflect a helix but are vital parts of many sheets, result in very different torsional characteristics from either of these extended structural types, helix or sheet. Thus they provide unique local singularities in the peptide conformation and consequently in its spectral behavior. Since they are ubiquitous elements of protein structures, their characterization has been a target of many studies [25,52,53,55,56]. We here report a systematic computational study of the IR and VCD spectral responses predicted for a variety of idealized turn geometries using the same level of density functional theory (DFT) spectral modeling we have employed previously for helix, sheet and hairpin structures [20,24,31,47,48,57–61]. Since the turn itself is a relatively small structure, essentially characterized with three amide links, we have looked at many variants with a full DFT approach (no fragmentation was used or needed [62]) and have investigated effects of basis set and solvation to a limited extent.

It should be clear that this is a modeling study, not an attempt to solve the structure of a specific sample. We rather seek to determine if there are any distinct spectral characteristics that can be associated with turns and if they can discriminate between geometries. Such small molecules would not have a well-defined structure in solution, so there is no realistic model system for experimental comparison. However, such turns are stable in larger systems, as characterized in hairpins and in cyclic peptides [52,53,55,56,63,64]. These modeling

computations do provide some bases for spectral simulations of such larger systems, which we have published and will report in the future [22,56,60,61]. It is this focused modeling of specific systems and structures, with an eye toward their applicability to larger, more structurally defined systems, that sets this work apart from the very nice studies of very small di- and tri-peptides that have generated some structural insight on those highly fluctional species with 2-D IR, Raman and other techniques as well as theory [11,23,65–68]. Many of these small structures have been modeled computationally as recently reviewed in great detail [66].

In our previous work, the characteristic spectral behavior of polypeptides arose from coupling of degenerate local transitions [20,24,31,47,48,57,58,60,61,69]. Accordingly, accuracy of the FF diagonal terms was originally of less concern since the important spectral characteristics originated in the off-diagonal terms. As these structural models were restricted to more realistic, shorter sequences, these degeneracies were lifted, but the basic coupling behavior still dominated the spectral response, although on a more local basis, resulting in broadened transitions and shifted frequencies. Similarly, while solvent effects were significant, vacuum calculations continued to have interpretive value, since the solvent-induced shifts were often uniform for these extended structures.

In contrast, the tight β-turn itself has no degenerate transitions, since each residue is different, so the diagonal terms become the dominant aspect of the turn spectral character. None-the-less, the relative dispersion for the diagonal contributions should remain the most important spectral characteristic for conformational studies, if one simulates the fundamental interaction of all the residues on the same basis. DFT calculations are typically in error by some margin, but for C=O groups, this error is often much larger, and as we [24,59,60,70–74] and others [27,28,37,66,74] have shown is often due to solvent interactions. Finding the proper correction for a uniform structure is less important, since the FF for all the residues are essentially in error by the same amount (diagonal contribution) and the computed frequencies could be shifted (scaled FF) to improve the match with experiment, if so desired. However, normally the issue is the relative dispersion of a single type of mode (e.g., the amide I) that can be used to characterize conformation. In a repeating structure this is due to interaction terms, off-diagonal FF, but in a β-turn the diagonal FF terms are all different, and, if the solvent correction is vital for getting a proper spectral representation, the errors will be different for different residues. Consequently, one cannot assume that there will be a uniform solvent shift for turn-containing structures, rather it is a behavior that needs testing. We must explore this question before reliable computational evaluation of turn spectral contributions can be successfully integrated with other structures such as helices and sheets. A recent example of this problem arising has been our efforts to simulate β-hairpin IR and VCD spectra, where sheet and turn segments are joined and both contribute to the spectra [60,61,63,75].

In this paper we begin the process of exploring IR and VCD of local peptide conformations by characterizing the isolated turn structures, exploring the variation in spectra that accompanies variation in conformation, basis set size and side chain (H $\rightarrow$ CH_3 or Ala $\rightarrow$ Pro) and, finally, modeling some of the solvent effects that might be expected. DFT modeling of the spectra allows us to assign turn-originating transitions and to develop a characteristic spectral response. Coupling turns to sheet strands to form hairpin structures has let us see how these spectral characteristics come out or are hidden for spectra of larger peptides of mixed conformation, but we will discuss such structures in detail separately [60,61,76]. We also do not directly address Raman spectra in this paper, but they of course depend on the same modes and FF interactions although different intensity mechanisms. Thus our focus will be on amide I and II modes which dominate the IR, with just brief mention of amide III modes which are weak in IR but relatively strong in Raman [77–79].

Methods

β-turn models

Idealized β-turn models containing the minimal number (3) of amide groups were constructed as various turn types with different sequences including: Ac-Ala-Ala-NMe (AA3), Ac-Aib-Gly-NMe (BG3) using the dihedral angles listed in Table 1. These structures were optimized with torsional constraints and were also fully optimized for comparison to see if the constraints imposed any significant spectral effects. These sequences were chosen for conformational simplicity and, in the case of BG3, for the ability to experimentally stabilize a turn structure [75,80]. A few calculations on different structures containing Pro, D-Pro and D-Ala residues (Pa3, pG3 and aa3, where lower case indicates D-resi-

Table 1 Dihedral angles for idealized β-turn geometries

Turn type	ϕ_{i+1}	ψ_{i+1}	ϕ_{i+2}	ψ_{i+2}
I (I′)	−60 (60)	−30 (30)	−90 (90)	0 (0)
II (II′)	−60 (60)	120 (−120)	80 (−80)	0 (0)
III (III′)	−60 (60)	−30 (30)	−60 (60)	−30 (30)

dues) were also done for comparison, since these sequences have also been employed to stabilize turns. The Pro models used ϕ, ψ angles derived from literature structures [81]. We have also computed IR and VCD spectra for 5- and 7-amide turns, Ac−$(Aaa)_n$−NMe, $n = 4$, 6, as well as larger β-hairpins which have been and will be reported separately [60,61,63,82].

Ab initio calculations

Most of our DFT-based ab initio calculations were done at the BPW91/6-31G** level in vacuum using the Gaussian 03 (or Gaussian 98) package of programs [83]. This somewhat simpler (non-hybridized) functional optimizes computation of the amide I and II modes, both in terms of frequency accuracy and speed of computation, but may not be optimal for lower frequency modes, should they be of eventual interest [57]. Various test calculations used larger basis sets (e.g., diffuse basis sets, 6-31++G**) and hybrid functionals (B3LYP). Some calculations used a conductor-like polarizable continuum model (CPCM or COSMO, [84,85]) correction for solvent effects, as implemented in Gaussian 03, or alternatively added an explicit inner shell of H-bonded water molecules to represent the major peptide-solvent interaction [24,60,63,70,71]. The general rationale for these calculations is to explore the spectral characteristics of a given structural type. Thus maintaining the chosen conformation is important. Consequently, these ϕ, ψ angles were initially constrained during the Gaussian minimization, while all the remaining structural variables were optimized by energy minimization before computing the force fields (FF) and atomic polar and axial tensors (APT and AAT). A number of calculations were done with full optimization, including the ϕ, ψ torsions, to test their relative conformational stability (in vacuum). The geometry was considered stable when the default Gaussian convergence criteria [83] were met. These calculations and structures investigated are summarized in Table 2.

To simulate spectra, atomic polar and axial tensors were then generated, combined with the normal mode displacements to generate a Table of dipole (D) and rotational (R) strengths. The AAT are needed for VCD simulation and are implemented in Gaussian 98 and 03 according to the magnetic field perturbation (MFP) theory developed by Philip Stephens [15,16,18] as enhanced by incorporation of gauge-independent atomic orbitals (GIAO) [19]. The final IR and VCD bandshapes for this discussion are obtained in all cases by summing over normal modes plotted with areas proportional to D and R, respectively, represented by constant width bandshapes, chosen to mimic typical peptide experimental properties. Computations were done on several different Linux-based PCs, either as part of a cluster or in the form of single or dual processor systems. For example, an Ac-Pro-Gly-NHMe minimization and FF calculation took ~32 h clock time on a 2.4 GHz Xeon (32 bit) processor with 2 GB of memory.

Table 2 Model structure designations, sequences, and conformational types studied

Peptide systems[a]	Geometries[b]	DFT method
BG3 (Ac-Aib-Gly-NMe)	I, II, III, I′ ,II′ , III′, I_{opt}, II_{opt}, III_{opt}, I'_{opt}, II'_{opt}, III'_{opt}, $I' + 7H_2O$,[d] $(I'_{opt})_{COSMO}$,$(II'_{opt})_{COSMO}$, $(III'_{opt})_{COSMO}$	BPW91/6-31G**, BPW91/6-31++G**, B3LYP/6-31++G**
AA3 (Ac-Ala-Ala-NMe)	I,II,III,I′,II′,III′, I_{opt}, II_{opt}, III_{opt}, $I'_{,opt}$, II'_{opt}, III'_{opt}, I_{COSMO}, II_{COSMO}, III_{COSMO}, $(I_{opt})_{COSMO}$, $(II_{opt})_{COSMO}$, $(III_{opt})_{COSMO}$, $(I'_{opt})_{COSMO}$, $(II'_{opt})_{COSMO}$, $(III'_{opt})_{COSMO}$	BPW91/6-31G**
aa3 (Ac-^{D}Ala-^{D}Ala-NMe)	I,II,III,I′,II′,III′	BPW91/6-31G**
Pa3 (Ac-Pro-^{D}Ala-NMe)	II-variant	BPW91/6-31G**, B3LYP/6-31+G**
pG3 (Ac-^{D}Pro-Gly-NMe)	1JY9, $1JY9_{opt}$[c]	B3LYP/6-31++G**, BPW91/6-31G**

[a] The number represents the number of amide groups in a structure

[b] The geometries without subscripts represent the structures obtained by optimization. To keep ideal turn geometries, four torsion angles (ϕ_{i+1}, ψ_{i+1}, ϕ_{i+2}, ψ_{i+2}) in two residues in a β-turn are constrained during optimization. The subscript 'opt' represents a fully optimized geometry via DFT calculation and the initial geometry is indicated. The subscript 'COSMO' represents an optimized geometry via CPCM option (solvent = water) in Gaussian program

[c] 1JY9 is the 20-mer hairpin structure from which the turn geometry is taken [81]. Two pairs of torsion angles for ^{D}Pro and Gly are (42°, 34°) and (58°, 42°), respectively

[d] '$+nH_2O'$ represents the explicit water model in which n water molecules, directly forming H-bonds to amide groups, are included for the minimal hydration of amide groups

Results

Structure and optimizations

The Ac-Aib-Gly-NMe (BG3) and Ac-Ala-Ala-NMe (AA3) sequences were tested for stability for three conventional turn types I, II and III as well as their inverse (mirror-image) conformations: I′, II′ and III′. Geometry optimization (all at the BPW91/6-31G** level) showed these I_{opt}, etc. structures to be quite close to the local minima as shown in Table 3. For BG3, the I_{opt} and II_{opt} ϕ_{i+1} and ψ_{i+1} values are very close to the starting type I and II values, while the ϕ_{i+2} and ψ_{i+2} values vary more, presumably due to the weaker conformational restriction of Gly as compared to Aib. Of course, since the BG3 residues are achiral, its standard and inverted, I, I′, etc., conformers are identical in energy though opposite in turn handedness (duplicate values not shown). A similar pattern of optimizing to a conformation near the "ideal" ϕ, ψ values during minimization is seen for AA3, in the case of the inverse turns, but the regular turn geometries change much more for the $i+1$ torsions, showing the effect of chiral interference. In vacuum, the type III conformer was converted to the type I minimum in each case, for BG3 and AA3, as seen in Table 3, but if the COSMO correction is included, the type I and III optimized structures are slightly different, but are qualitatively quite similar. This pattern of type III structure being favored by COSMO relative to the vacuum was previously found in our full optimization of helical deca-peptides (Ac-$(Ala)_9$-$NHCH_3$) where a 3_{10}-helical structure was the minimum energy helical structure favored for computations with COSMO corrections [36]. Clearly, if there are two separate minima, the barrier between them must be small. It is interesting that the type I geometry is lowest in energy overall for the chiral AA3 sequence while the type II′ geometry is lowest among the inverted geometries, and in vacuum is more favored than the regular type II form. For the BG3 and AA3 sequences, the type I(I′) is lower in energy, even with COSMO, but the BG3 difference in vacuum is too small to be reliable.

Spectral results

The computed amide I and II (N–H on amide) IR and VCD spectra for BG3 at various DFT levels are summarized in Table 4. In each case the three amide I modes are relatively dispersed over $\sim 25\,cm^{-1}$ with two of them higher (clustered), the lower of the three is the C = O

Table 3 Backbone torsion angles and relative energies for optimized β-turn structures

Peptide	Geometry	ϕ_{i+1}	ψ_{i+1}	ϕ_{i+2}	ψ_{i+2}	Relative energy (kcal/mol)[a]
BG3	I'_{opt}[a]	64	27	105	−18	0
	II'_{opt}	55	−126	−107	21	0.26
	III'_{opt}	64	27	105	−18	0
BG3	$(I'_{opt})_{COSMO}$[a]	56	37	94	−8	0
	$(II'_{opt})_{COSMO}$	56	−128	−89	9	1.91
	$(III'_{opt})_{COSMO}$	58	31	77	8	0.67
AA3	I'_{opt}[a]	63	29	67	17	4.04
	II'_{opt}	57	−127	−108	20	1.73
	III'_{opt}	63	29	67	17	4.04
	I_{opt}	−79	−4	−108	14	0
	II_{opt}	−66	119	73	16	2.50
	III_{opt}	−79	−4	−108	14	0
AA3	$(I'_{opt})_{COSMO}$[b]	56	39	71	6	2.02
	$(II'_{opt})_{COSMO}$	58	−125	−103	17	1.72
	$(III'_{opt})_{COSMO}$	58	34	63	23	2.52
	$(I_{opt})_{COSMO}$[b]	−65	−29	−94	7	0
	$(II_{opt})_{COSMO}$	−64	128	63	22	1.91
	$(III_{opt})_{COSMO}$[b]	−65	−29	−79	−9	0.88

Optimized geometries were obtained by starting from ideal turn structures and minimizing the energy via DFT BPW91/6-31G** calculations. Calculations with the COSMO model are indicated in the subscripts

[a] The energies of optimized structures are compared among the turns with the same sequence and with the same solvent model. The lowest energy structure is assigned with 0, and other energies are relative values

[b] Optimizations with these geometries with COSMO model were not converged with the default convergence criteria (the others converged well). A minimum energy, metastable structure was taken as an approximate optimized geometry, since the vibrational frequencies did not change further

Table 4 Functional and basis set dependence for BG3 amide I and II in type I′ turn

DFT level	Frequency, ω[a] (cm^{-1})	IR, D ($debye^2$)	VCD, R ($\times 10^{-6}$ $debye^2$)	Amide groups coupling[b]
BPW91/6-31G**	1,730	0.042	0.28	$(i+1)$, i_{oop}, CH_2
	1,728	0.055	1.14	i, $(i+1)_{ip}$, CH_2
	1,702	0.063	−1.87	$(i+2)$
	1,519	0.042	−0.06	$(i+2)$, $(i+1)_{oop}$
	1,485	0.057	1.74	$(i+1)$, $(i+2)_{ip}$, i_{oop}, CH_2
	1,470	0.041	0.24	i, $(i+1)_{ip}$
BPW91/6-31++G**	1,704	0.053	1.32	$(i+1)$, CH_2
	1,694	0.068	0.81	(i+2), i_{oop}, CH_2
	1,677	0.078	−2.61	i, $(i+2)_{ip}$
	1,518	0.041	0.01	$(i+2)$, $(i+1)_{oop}$
	1,485	0.054	1.80	$(i+1)$, $(i+2)_{ip}$, i_{oop}, CH_2
	1,467	0.044	0.19	i
B3LYP/6-31++G**	1,753	0.058	1.58	$(i+1)$, CH_2
	1,740	0.053	1.39	$(i+2)$, i_{oop},, CH_2
	1,729	0.099	−3.54	i, $(i+2)_{ip}$
	1,571	0.052	−0.17	$(i+2)$, $(i+1)_{oop}$
	1,540	0.063	2.14	$(i+1)$, $(i+2)_{in}$, i_{oop}, CH_2
	1,521	0.044	0.14	i, $(i+2)_{ip}$

[a] Methyl hydrogens were deuterated to avoid mixing with the amide II

[b] Mode is described with indices of a contributing residue and the phase relation. $i+1$ and $i+2$ are two residues forming the tight β-turn, ith C=O originates from N-terminal acetyl group. CH_2 indicates the scissor motion at C_α of Gly. The order of indices indicates the relative magnitude of contribution such that the largest motion is first and the next, second, etc. The subscript represents the phase of the motion with respect to that of the first, most intense one

involved in the H-bond (Ac C=O to Gly N-H). The H-bond formation lowers the frequency as compared to the vacuum, unbound C = O groups. The clustering of the high frequency amide I modes is more but the dispersion is the same for the 6-31G** as compared to the 6-31++G** basis set and more for BPW91 than B3LYP functional. This may speak to a difference in coupling for the various FF, but the intensity patterns show no qualitative difference. N-deuteration has little qualitative effect on the amide I′ as well. The amide II modes have even larger dispersion ($\sim 50\,cm^{-1}$ in each case) and just the opposite ordering since the high frequency mode is different, due again to its H-bond (Gly N-H), which increases the amide II frequency by restricting bending motion. However, solvation would affect these non-H-bonded modes more than the cross strand ones. Since these turn geometries do not repeat in sequence and thus do not gain intensity by coupling to near-degenerate modes, these small deviations would have little detectable spectral impact.

The variation of amide mode frequencies with change of method follows our previous observations for test molecules [70,86] in that the use of 6-31++G** basis set with the BPW91 functional reduces the predicted amide I and II frequencies by about $30\,cm^{-1}$, making them approach a region just above the experimentally observed values. However, use of the B3LYP functional makes the agreement worse. More importantly, use of BPW91 and 6-31++G** reduces the separation of the amide II and amide I modes (change in the right direction). The amide I–II gap is much too large in all these calculations, since from experimental observation, it should be of the order of $100\,cm^{-1}$ in solution. Even if one corrected for the absolute frequency error with a scale factor, the result still would have too much amide I–II separation suggesting that some sort of explicit solvent correction is needed for this aspect of the spectral modeling. This has of course been addressed by several groups [24,70–72,74,82,87].

The results for type I, II and III ideal turn geometries with the BG3 sequence are enumerated in Table 5 at the BPW91/6-31G** level of calculation. The clustering of amide I and II modes again reflects the H-bond formed from the Ac C=O to Gly N–H remains in all the turn types; however, the amide I for type II shifts more than for the other two, resulting in more dispersion for this turn type. Such a frequency shift, perhaps reflective of H-bond strength, would discriminate between these turns, but if they were part of a larger β-hairpin [53,63,75,88–90], the β-strand modes would obscure the low frequency turn contribution. Isotope labeling might be a way to identify these singular modes [22,61,75], but our initial attempts to label the turn H-bond C=O have not been simple to interpret [76]. The VCD patterns

for the type I and II amide I mode do differ with the center component being positive for type II and negative for type I, and the type II VCD is much weaker, but both would be hard to detect in a real molecule with broadened bandshapes (see Fig. 1). The amide II mode IR differs in that type II has less dispersion than the other two, and the VCD in type I is mostly negative while type II has a dominant central feature that is positive. This amide II VCD sign variation is the largest difference between types I and II. (Further, if we go on to consider the amide III, since it is complementary to the amide II, having the opposite phase of internal C–N and N–H motions, it is not surprising that the amide III for type I is predicted to be opposite in sign to that of the amide II, but for type II the situation is less clear, as described in a later section below.) Type III has an amide I VCD pattern similar to type II, but a different amide II VCD, being all negative, closer to type I (recall Fig. 1 is for type I′ and III′, so these features are positive). It should be noted that type III turns are the building blocks of 3_{10}-helices, and the characteristic 3_{10}-helix amide II VCD is an intense, relatively sharp, negative band centered on the absorbance [31,33–35]. It is important to realize that in these calculations the C_α-H scissor motion on the Gly residue can overlap amide II (to the low energy side). This can lead to some mixing in the computed spectra that is probably over-emphasized as compared to experimental results for real turns since, for this DFT level and in vacuum, the amide II modes are computed too low in frequency and the CH_2 scissor mode too high. This is normally not a problem in our spectral modeling since only Gly has such a scissor mode, and most structures have only a few Gly residues. For this study of turns, the CH_3 modes, which also would partially overlap the amide II in the computed spectra, have been spectrally eliminated by computer conversion to CD_3. Finally, small differences between Tables 4 and 5 can result from the use of an ideal model built without torsional optimization, so that I and I′ are not precise mirror images. However, the VCD are opposite in sign as expected.

Table 5 Amide I and II predictions for BG3 ideal turns at the BPW91/6-31G** level

Turn type	Frequency, ω[a] (cm^{-1})	IR, D ($debye^2$)	VCD, R ($\times 10^{-6}$ $debye^2$)
I	1,730	0.042	−0.29
	1,728	0.055	−1.11
	1,702	0.063	1.86
	1,519	0.042	0.06
	1,485	0.057	−1.74
	1,470	0.041	−0.25
II	1,726	0.056	−1.15
	1,724	0.041	0.96
	1,686	0.065	0.87
	1,519	0.053	−1.34
	1,490	0.041	1.32
	1,486	0.045	0.43
III	1,734	0.059	−2.47
	1,730	0.029	0.92
	1,703	0.062	1.54
	1,520	0.039	−0.36
	1,484	0.051	−0.89
	1,471	0.047	−0.21

[a] Methyl hydrogens are deuterated

These results are summarized graphically in Fig. 1 for ideal types I′, II′ and III′. A comparison is also made there for two calculational levels, B3LYP/6-31++G** (red) versus BPW91/6-31G** (black). In this case, due to the overlap of component bandshapes, a fairly consistent pattern is seen with the two basis set/functional results, resulting in predicted spectra that are just shifted in frequency. The IR absorbance differences are basically due to the overlap (less with the 6-31++G** basis) of the two non-H-bonded amide I modes. While the amide I shapes are basically the same for the IR of all three turns, with a bit more apparent dispersion (band width) for the type II′ due to its lower H-bonded C=O mode, there are real differences in the VCD. Although the VCD sign patterns are stable with variation in basis set, the intensities do change making the type II′ much weaker than the types I′ and III′. All the turn types have a negative couplet for the amide I VCD, which is opposite the Table 5 values since the turns in the figure are left-handed. In contrast, the amide II difference is evident in terms of the net overall intensity in the band being positive for type I′ and negative for type II′, effectively discriminating between these two types. The type III′ VCD is qualitatively like the type I′ aside from amide II relative intensity, which is FF sensitive. So while the bandshapes vary qualitatively with basis and functional, this is a minor discriminator since these FF effects mostly impact frequency. Thus, VCD offers the only hope of reliably discriminating between turn types in these modes, and then only between types I and II, since the IR differences are too subtle. The question remains how sensitive are the differences to structural variation in a real turn, how will these local turn modes couple to other peptide modes, and which of this character will remain in a larger peptide. It can be noted that the VCD for a 3_{10} helix has a positive couplet amide I and a sharp negative amide II [31,35], both of which are opposite to the results in Fig. 1f, which is correct since the 3_{10} helix is composed of type III turns, as opposed to the mirror image versions in Fig. 1.

For the AA3 sequence there is an energetic and consequently a frequency difference between the left- and right-handed turn conformations, due to the chirality at

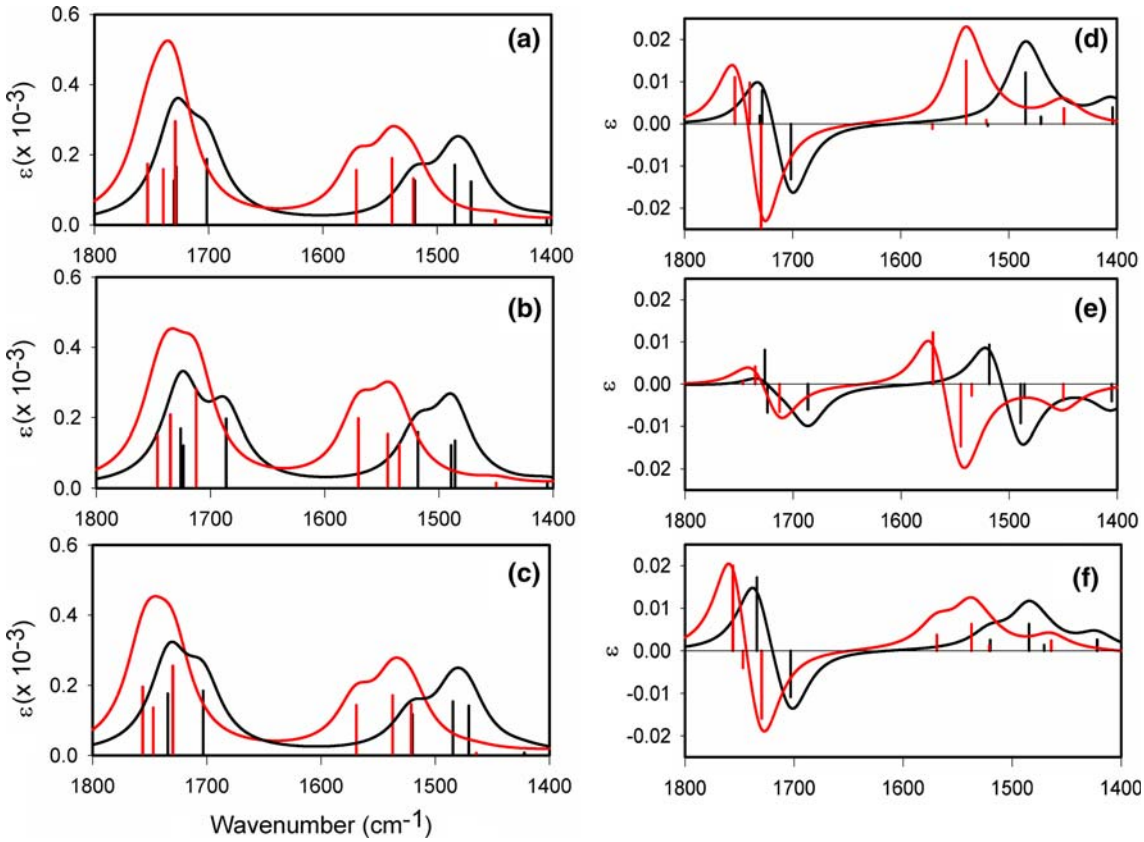

Fig. 1 Comparison of DFT theory predicted amide I and II IR and VCD spectra for the BG3 sequence (vacuum) in three idealized turn types: type I′ (**a**), type II′ (**b**) and type III′ (**c**) with **d**, **e** and **f** showing the corresponding VCD spectra. Method used: B3LYP/6-31++G** (*red*) versus BPW91/6-31G** (*black*). *Note*: additional bands close to the amide II (1,400–1,450 cm^{-1}) are due to the Gly CH_2 scissor mode

C_α, as summarized in Table 6. For the type I and III amide I, these appear to be relatively minor effects, and the IR intensity patterns are about the same for both, and for VCD the type I, I′, etc. are opposite in sign, of course. The VCD intensities do vary quite a bit, showing that to be the more sensitive measure of conformational variation. However, for the type II the nature of the modes appears to have changed, and the sign pattern for standard and inverted turn is the same for amide I, but with quite different intensity patterns, and are opposite, as expected, for amide II. The amide I has a dispersion of about 30 cm^{-1} except for type II, II′ where it is $\sim 40\,cm^{-1}$ due to the lower frequency H-bonded C=O mode, much as seen for BG3. The biggest amide I difference is again the weak magnitude of the type II VCD. The amide II mode IR and VCD are also similar for I and I′, etc. but do vary more because of the coupling to lower energy modes affected by the residue chirality. The dispersion difference for type II is less significant than for BG3.

Unconstrained optimization of these structures in vacuum basically eliminates the need to discuss the type III or III′ turns, since in our hands these all convert to type I or I′. With COSMO optimization there is a difference, but the end results for I_{COSMO} and III_{COSMO} are quite similar. In general, the changes in the optimized predicted spectra are not very big, but are somewhat different for type I, II and type I′, II′. It is easiest to just compare them graphically with results for the constrained conformation (see Fig. 2). The VCD stays also about the same aside from variation in magnitude. The sign of the type II and II′ amide I VCD does not change after optimization, but the type II′ intensity (Fig. 2e) is higher than type II (see Fig. 3e, black). The main type I′ type III′ difference is in the amide II, which is more disperse for type I′.

Another interesting stereochemical interaction to consider is the impact of opposite enantiomer residues, such as D-Ala (indicated as (**a**)). While one might expect the spectra of type I for aa3 to be the same as type I′ for AA3, type I of each is not the same. These are compared in Fig. 3 along with BG3 for types I, II and III. At some level the BG3 comparison allows separation of residue from conformational effects. For clarity the

Table 6 Amide I and II *D* and *R* values for AA3 ideal turns

Standard geometry				Inverted geometry			
Type	Frequency, ω[a] (in cm^{-1})	IR, *D* (in $debye^2$)	VCD, *R* ($\times 10^{-6}$ $debye^2$)	Type	Frequency, ω[a] (cm^{-1})	IR, *D* (in $debye^2$)	VCD, *R* ($\times 10^{-6}$ $debye^2$)
I	1,735	0.049	−1.15	I′	1,738	0.046	1.05
	1,716	0.041	−1.05		1,718	0.043	0.61
	1,706	0.070	1.11		1,707	0.063	−2.71
	1,513	0.054	−0.12		1,518	0.049	−0.74
	1,484	0.070	−1.55		1,495	0.050	3.30
	1,472	0.031	−0.86		1,480	0.023	−0.23
II	1,735	0.037	0.09	II′	1,728	0.048	0.96
	1,716	0.048	−0.38		1,715	0.048	−0.52
	1,689	0.068	−0.20		1,691	0.064	−1.06
	1,519	0.058	−1.61		1,517	0.066	1.13
	1,494	0.041	2.71		1,501	0.027	−0.90
	1,487	0.035	0.42		1,484	0.044	−0.78
III	1,737	0.047	−2.02	III′	1,731	0.043	1.65
	1,726	0.040	0.02		1,723	0.038	−0.22
	1,707	0.065	0.55		1,708	0.058	−2.13
	1,511	0.048	−0.50		1,513	0.051	0.26
	1,478	0.072	−0.10		1,490	0.049	0.14
	1,471	0.035	−1.48		1,483	0.023	0.01

[a] For each type turn, from the highest frequency, three amide I and next three amide II modes are listed; methyl hydrogens deuterated

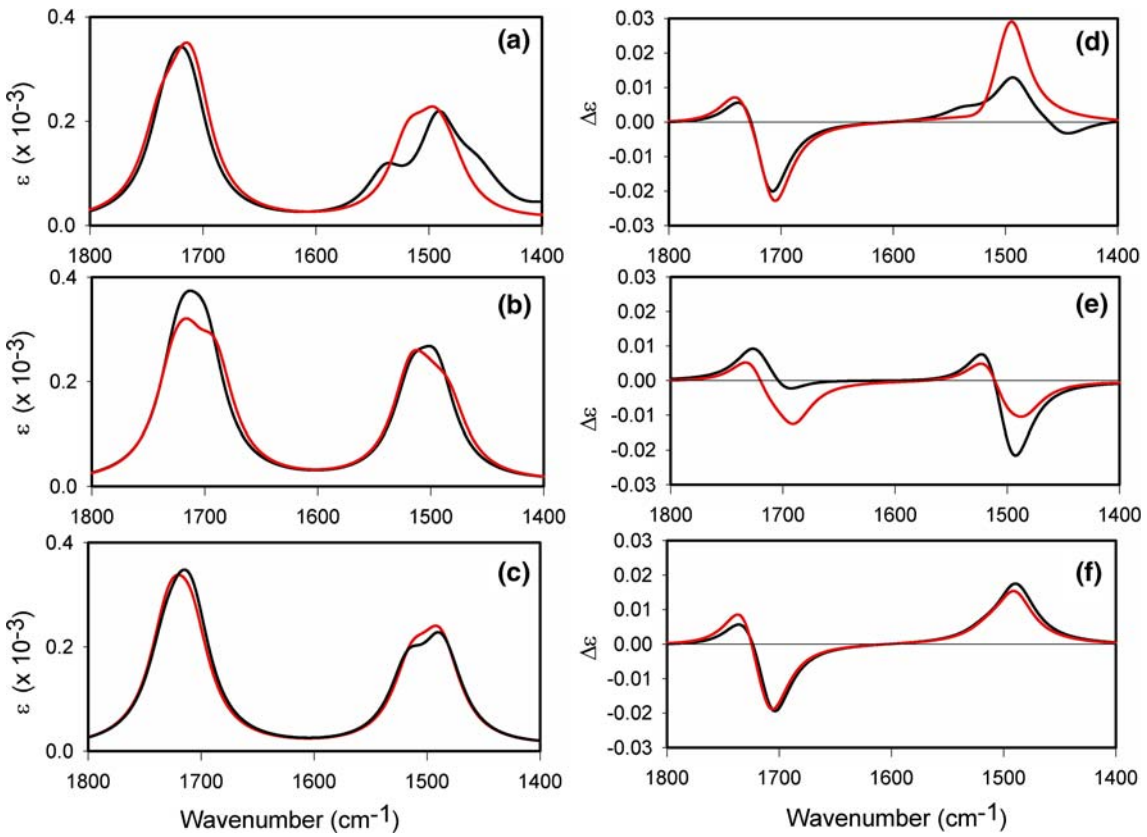

Fig. 2 Amide I and II (IR and VCD) predicted spectra of AA3 turns for ideal (*red*) and fully optimized (*black*) inverse turn geometries, computed at the BPW91/6-31G** level. **a**, **d** IR and VCD for type I′, respectively, **b**, **e** are for type II′, **c**, **f** are for type III′

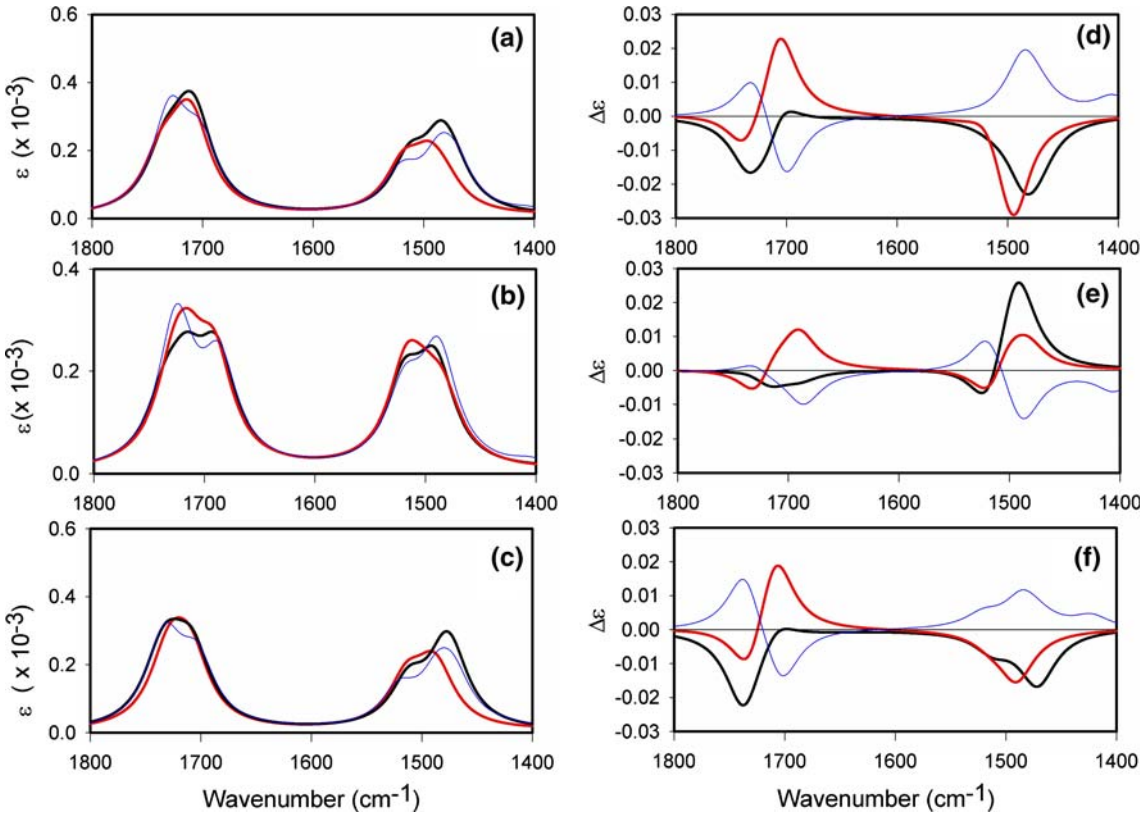

Fig. 3 Predicted IR (**a**, **b**, **c**) and VCD (**d**, **e**, **f**) of ideal geometry type I (**a**, **d**), II (**b**, **e**) and III (**c**, **f**) turns for AA3 (*black*), aa3 (*red*) and types I′, II′ and III′ for BG3 (*blue*), at the BPW91/6-31G** level

BG3 are plotted as the inverse turns (blue), resulting in opposite sign patterns for VCD (less overlap confusion) from those of type I aa3 in the amide I. The BG3 turns have even better mirror imaging of the VCD for all types in aa3 (red) than in AA3 (black) in the amide I. The aa3 has less dispersion and more variation in intensity in the amide II and does not have the type II amide I VCD sign problem. The source of this inconsistency is hard to determine, since the three amide I modes are uncoupled in both type II cases, being localized on the center, C- and N-terminal amides in order of decreasing frequency.

One method for stabilizing a turn is to use Pro as one residue due to its restriction in the ϕ torsion. In particular, the D-Pro-Gly sequence has been shown to develop exceptionally stable turns and to initiate hairpin formation [63,64,81,91,92]. In Fig. 4 are compared IR and VCD computed at BPW91/6-31G** and B3LYP/6-31++G** levels for pG3 both fully optimized and torsionally constrained (to the PDB: 1JY9 structure) [81]. These structures form very distorted analogs of a type III′ turn, with the optimized structure somewhat closer to a type I′ turn (Tables 1, 2). The characteristic low frequency amide I for the Ac-^{D}Pro linkage consistently appears below the others in the IR, as seen experimentally [63]. Optimization does bring the Ac-Pro C=O closer to the other amide I bands. Changing basis sets has the main attribute of lowering the amide I and II gap, but surprisingly, this comes about by raising the amide II frequency with little impact on the amide I. The amide I frequency does not come down significantly because the basis set advantage is offset by increased error from use of the B3LYP functional. The VCD for these pG3 structures is a bit more intense than for the AA3 above, but the amide I in particular is quite unstable, seemingly changing sign with optimization and with basis set. The ideal structures tend to have the center and C-terminal amide C=O modes mixed (in-phase for highest frequency), but the low frequency N-terminal Ac-Pro amide mode is not coupled in. On minimization the modes become less coupled and more localized. This suggests that by becoming more separated, the cross-branch H-bonded C=O is less well coupled to the structure and may distort more with optimization or other variation. On the other hand the amide II is quite stable among all the variations presented.

The Pa3 variant in contrast optimized to almost an ideal type II turn whose amide I spectra (see Fig. 5)

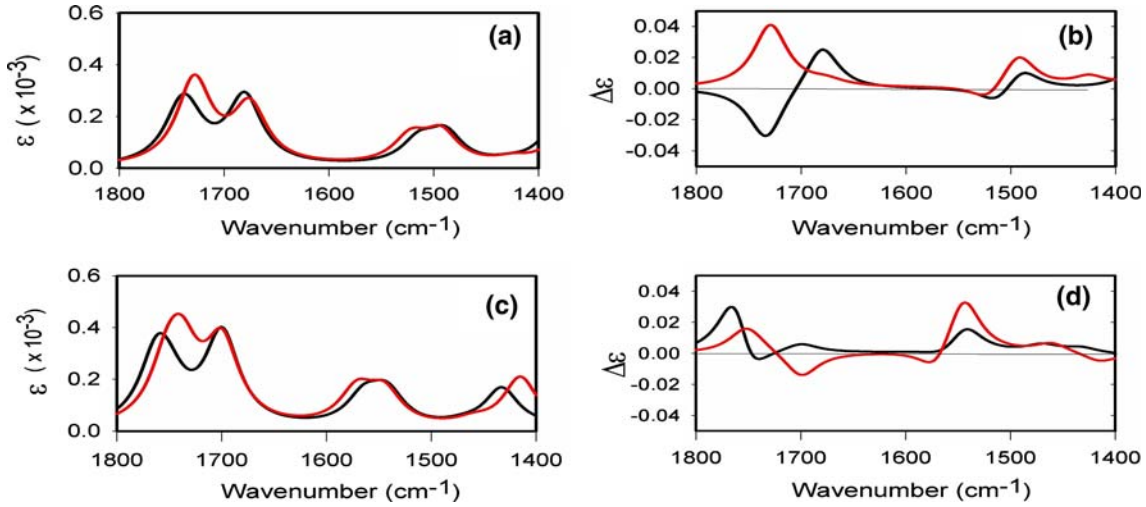

Fig. 4 Predicted IR and VCD of pG3 for the constrained geometry (PDB: 1JY9) model hairpin peptide (*black*) and the fully optimized geometry (*red*). BPW91/6-31G** calculations are presented in **a** and **b**, and B3LYP/6-13++G** are in **c** and **d**. The lower modes (1,400–1,450 cm^{-1}) are CH_2 scissor modes

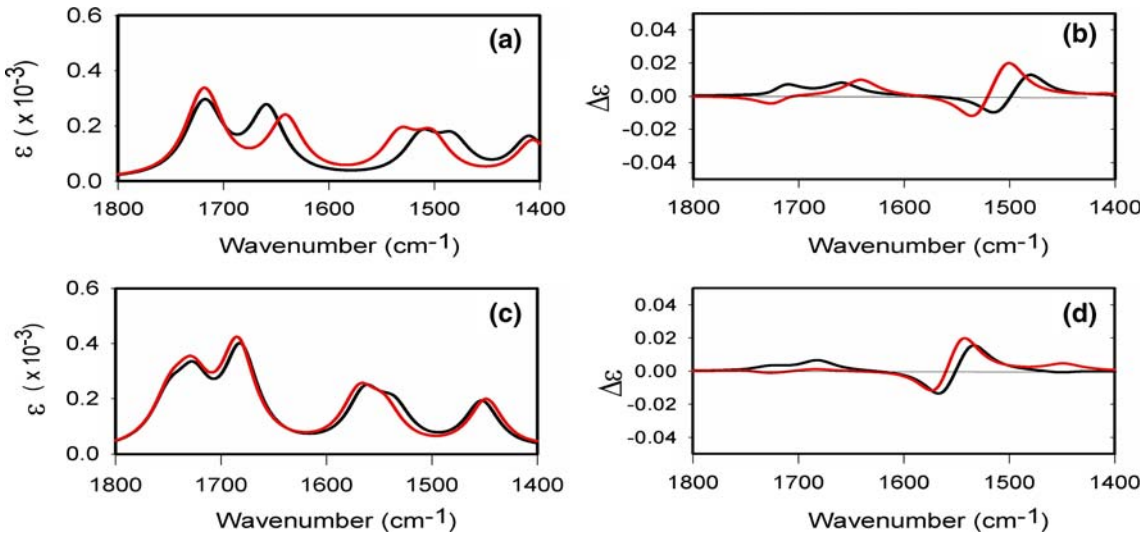

Fig. 5 Predicted IR and VCD of Pa3. The results of the model geometry in which torsion angles at $i+1$ and $i+2$ residue are fixed with type II turn but ϕ_{i+1} is optimized as shown with a *black line*, and the results of a fully optimized geometry are shown with a *red line*. BPW91/6-31G** calculations are presented in **a** and **b**, and B3LYP/6-31+G** are in **c** and **d**

have similar stability problems with change in basis set, but there the amide I VCD signal is exceptionally weak. However, its amide II is more consistent and, somewhat surprisingly, reflects the amide II found for pG3, including the increase in frequency for spectra computed with basis sets containing diffuse functions. The amide II VCD of both peptides have the same sign pattern, essentially because type I and II have opposite sign VCD in the amide II (see Fig. 1), and here pG3 is a distorted inverse turn (I′ or III′) while Pa3 is essentially type II.

Solvation can have a major impact on amide I frequencies in particular. We attempted to model this interaction both by inclusion of explicit waters of hydration and with the polarizable continuum model, COSMO. As we and others have shown [70,87], inclusion of an inner shell of water and then surrounding that with a dielectric model (e.g., PCM approach) is an even better method for accurate frequencies, but obviously that is more computationally demanding. We did not include such models in this broader survey test of turns, since the likelihood of transferring it to larger structures is

Table 7 Hydration effects on amide I and II spectral parameters for type I′ BG3

Method	Frequency, ω[a] (cm^{-1})	IR, D ($debye^2$)	VCD, R ($\times 10^{-6}$ $debye^2$)	Amide group couplings[b]
Vacuum	1,730	0.042	0.28	$(i+1)$, i_{oop}, CH_2
BPW91/6-31G**	1,728	0.055	1.14	i, $(i+1)_{ip}$, CH_2
	1,702	0.063	−1.88	$(i+2)$
	1,519	0.042	−0.06	$(i+2)$, $(i+1)_{oop}$
	1,485	0.057	1.74	$(i+1)$, $(i+2)_{ip}$, i_{oop}, CH_2
	1,470	0.041	0.24	i, $(i+1)_{ip}$
Minimal hydration	1,691	0.066	1.61	$(i+1)$, CH_2
($BG3+7H_2O$)	1,666	0.066	0.21	i, $(i+2)_{oop}$, CH_2
BPW91/6-31G**	1,648	0.113	−2.15	$(i+2)$, i_{ip}, CH_2
	1,548	0.051	1.56	$(i+2)$, i_{ip}
	1,538	0.027	−2.55	i, $(i+2)_{oop}$, $(i+1)_{oop}$
	1,505	0.055	4.44	$(i+1)$, i_{ip}, $(i+2)_{oop}$, CH_2
COSMO	1,679	0.094	2.93	$(i+1)$, $(i+2)_{ip}$, CH_2
BPW91/6-31G**	1,672	0.104	−1.36	$(i+2)$, $(i+1)_{oop}$, i_{oop}, CH_2
	1,651	0.116	−2.97	i, $(i+2)_{ip}$
	1,525	0.078	1.71	$(i+2)$, $(i+1)_{ip}$, i_{ip}
	1,505	0.083	−2.40	i, $(i+1)_{oop}$
	1,487	0.066	3.96	$(i+1)$, i_{ip}, $(i+2)_{oop}$, CH_2

Comparison of explicit and COSMO implicit water calculation
[a] Methyl hydrogens are deuterated
[b] Mode description follows that described in Table 4

remote, and realistic solvent models must account for dynamics, as is being done in various labs [71,74]. Fluctuation of the peptides is also a dynamic problem better addressed using MD of realistic structures, such as hairpin sequences one can study experimentally. [61]

The impact of solvent is to lower the amide I frequency closer to the experimental region and to raise the amide II frequency, as shown in Table 7 for type I′ of BG3. With the explicit water calculation, the critical amide I–II separation is brought into a realistic range. The IR intensities increase with solvation, as is typical of H-bonding to a C=O group, but the VCD increase is less, which might suggest that dipole coupling is not the only intensity mechanism. The VCD sign pattern is preserved (compared to Fig. 2), but the amide II shifts component bands about. For the COSMO correction there is less amide I dispersion, but the amide I–II gap is larger and the IR amide I and II intensities are higher than with explicit water (explicit water leads to more dispersion, but COSMO to compression). Thus while much more difficult to compute, the explicit water calculations give results more easily interpreted with regard to experimental frequencies. However, from a practical basis, the COSMO correction provides results in a realistic frequency range and, since it is normally an easier calculation, COSMO poses an attractive, approximate alternative. In our hands geometry optimizations were not as stable with COSMO since the minimum energy was not achieved with a zero gradient, implying the surface is not sufficiently smooth. Fortunately, the geometry and force field converged to values close enough to the minimum that the numerical instability did not affect our result. For type I′ the VCD pattern is preserved while being shifted to the more realistic frequencies obtained from both explicit water and COSMO calculations, but the amide II has more variation, presumably due to the explicit forces on N–H bends caused by directional H-bonds to water. This is most easily seen in Fig. 6, where the two solvent corrected spectra are compared with the vacuum results.

The discussion above has focused on the amide I and II modes since they dominate IR and VCD analyses of peptides. The amide III mode has been the target of some protein and peptide IR studies [77,93,94], but is very weak and dispersed by interaction with other modes. However, it is also very useful for Raman analyses since it has large frequency shifts with structural change (helix to sheet, in particular) [4,11,12]. Our simulations, of course, predict frequencies and IR and VCD spectra for the amide III, and those frequencies are of course the same as would be seen in the Raman, so some comments are in order. The amide III mode and the CαH wag mix to varying degrees, which is conformationally dependent and is probably the source of its structural sensitivity. This is quite FF sensitive, and in our tests was best seen for the COSMO optimized structures when the methyl groups were H/D exchanged. As shown in Fig. 7, these amide III modes are also computed to be

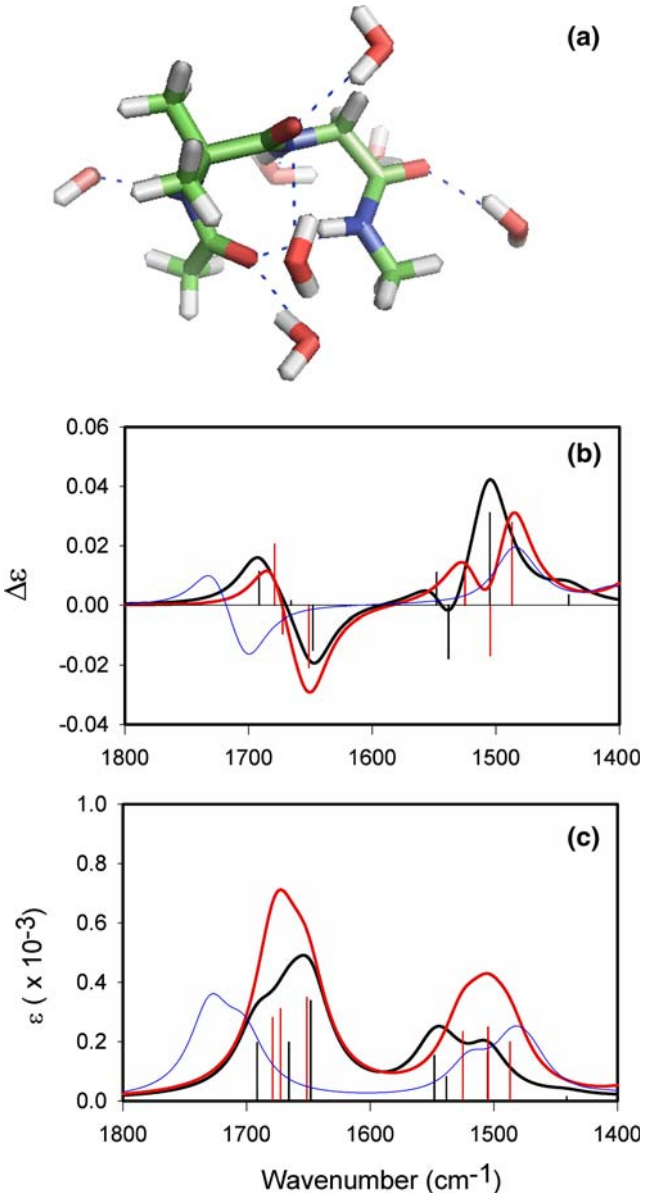

Fig. 6 Comparison of solvent effects. Amide I and II modes of BG3 type I′ geometry simulated with explicit water as BG3 + $7H_2O$ (*black*), as BG3 with COSMO (*red*) and for BG3 in vacuum (*blue*), computed at the BPW91/6-31G** level. The minimal hydration structure obtained after minimization is shown in **a**. Plots **b** and **c** are VCD and IR, respectively. The picture was made with PyMOL (www.pymol.org)

quite weak and broad in the IR, with the CαH modes being at $\sim$1,300 cm^{-1} and the N-H deformation (amide III) at about 1,250–1,200 cm^{-1} in vacuum. However, for the COSMO optimized structure and FF the amide III and CαH become more mixed in the 1,300–1,200 cm^{-1} region. The result for IR is an increase in intensity (but less than for the amide I and II, which nearly doubled in COSMO). For VCD a stable spectral pattern is seen. All the type I amide III VCDs have broad positive band (negative for type I′) over the entire region, as do the type III. The type II differs in having almost no amide III VCD. This is consistent with helical studies which show a broad positive VCD for α-helices and 3_{10}-helices, yet little signal for random coil peptides (locally 3_1-helices) [20,57,77]. Since the type III turn mimics the 3_{10}-helix the best, this is an observation consistent with our calculations, and with previous helical calculations [36].

Discussion

This paper explored the computational effects of basis set, functional, geometry, optimization, turn type and solvation for simulating IR and VCD of type I, II and III β-turns and their inverted conformers for a few different sequences. The computational methods used depend on those developed by Philip Stephens and co-workers over the last decade. The advances we have made in interpreting peptide IR and VCD in high detail for many conformations are dependent on the advances in computational spectroscopy made possible by his research and incorporated into available software packages, such as Gaussian 03 [15,16,18,19,83,95,96]. Our work is primarily directed at finding reliable interpretations of spectral responses in terms of structure for experimentally realizable peptide systems. Small peptides have little stable structure that one can analyze unless a molecular dynamics approach is taken. However many large peptides have moderately stable structures (aside from the termini) that can be computationally modeled. We are primarily interested in hairpins as elements of β-sheets, so the blocked turns discussed in this manuscript are potentially relevant to analysis of their spectra. Zwitterionic structures, as studied by others focusing on amino acids and very small peptides, may be of interest for other purposes, but would not appropriately model the turn in a hairpin, which obviously must be covalently bound to the β-strands. Thus we have not considered them or their literature, which has been reviewed recently by Jalkanen [66].

For these amide focused calculations, there is no advantage to use the hybrid B3LYP functional at the harmonic level. Its more complex nature slows down the calculations but offers no improvement of (actually degrades) the frequency patterns, as we have demonstrated repeatedly here and in our previous work. On the other hand, use of a basis set with diffuse functions does have a positive impact on the frequency distribution, but it costs considerably more in time and memory and only results in limited improvement (see Fig. 1;

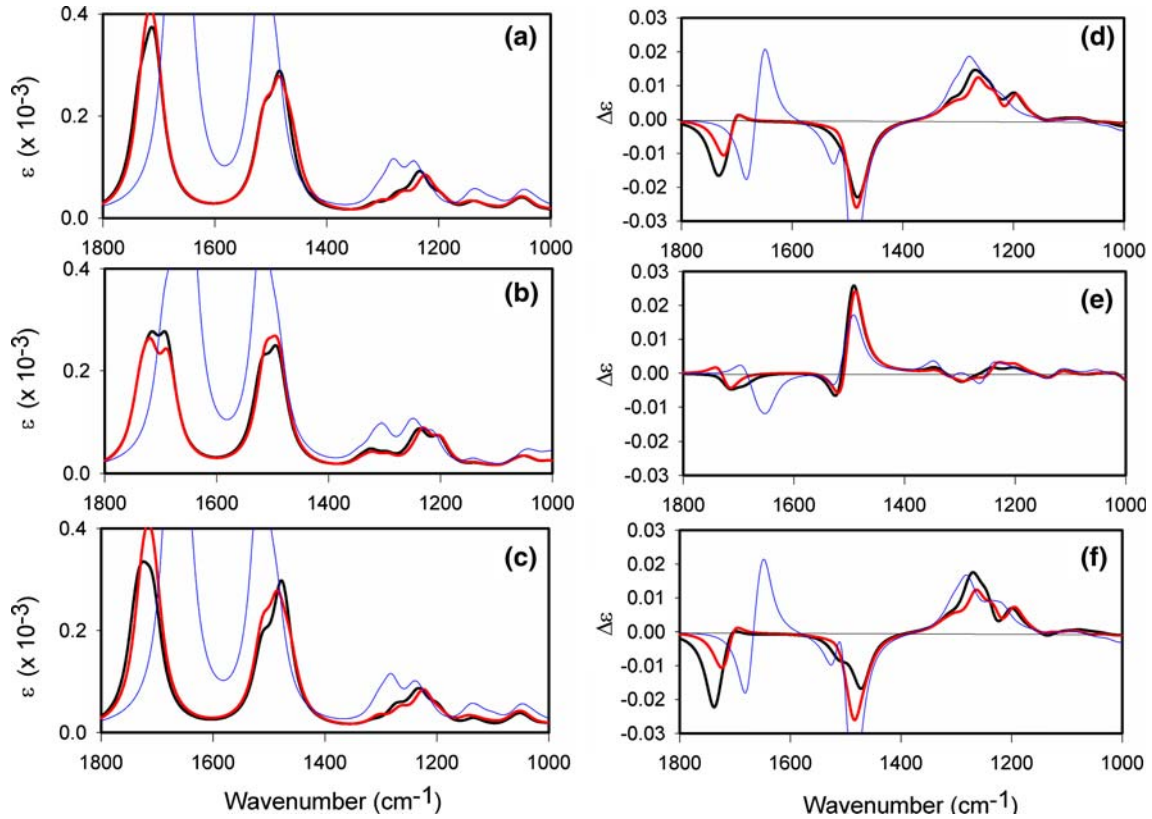

Fig. 7 IR (*left*) and VCD (*right*) spectra including the CαH and amide III modes (amide I and II are also shown) computed for AA3 with BPW91/6-31G** and for all methyl hydrogens deuterated. **a**, **d** type I, **b**, **e** type II and **c**, **f** type III. *Black lines* represent ideal and *red* the fully optimized geometries. *Blue lines* represent the common turns (Type I, II and III) with COSMO optimization and constrained torsions

Table 4). For example, in the Pa3 calculations, BPW91/6-31++G** and B3LYP/6-31++G** (vacuum) computations were 39 and 68 h on a four processor computer, respectively, while for 6-31G** (eliminating the diffuse functions) they were 8.5 and 12.3 h, about four times faster. An alternate correction can be obtained by simulating the solvent effect. Use of explicit water is the best such method to account for solvent, even with a smaller basis set, but one must assume a structure that certainly is a very crude approximation to the dynamic fluctuation of the water molecules in a room temperature solution. In contrast, the COSMO correction does a fair job. In the end the bandshapes are preserved but the frequencies are better with some sort of solvent correction. This is a diagonal FF effect, one that does not impact the off-diagonal interaction terms much at all, which is demonstrated here by the preservation of VCD shapes and signs. This has been shown explicitly in QM-based isotope labeling computations for defined structures which also compared them with experimental results [24,60,61]. Others have used empirical coupling parameters to get approximate measures of isotopic label coupling in a variety of structures [23,27,28,67,97–100]. Thus, the careful use of vacuum calculations with modest basis sets (6-31G**) can yield spectra which have known flaws, but ones for which we can compensate [71,86]. This then allows larger problems to be attacked at a higher computational level.

On the other hand, COSMO does influence minimization and relative energies. Unfortunately, in our hands these minimizations are also a bit unstable. The type I and III turns have very similar optimized structures with COSMO, though not identical, which is the case in vacuum. For BG3, otherwise achiral, type I is favored and for AA3 the same is true, but for the inverted turns, type II′ is lower in energy than type I′. In this case the COSMO correction parallels the vacuum result. These energy differences are modest so that binding to β-strands, alteration of side-chains or inclusion of a complete water environment could clearly change them. Thus both structures appear to be energetically accessible to the peptides, with our results only indicating isolated propensities for type I or type II′ in AA3, and perhaps type I (I′) for BG3.

In the model calculations we have shown that the standard turn types have very similar amide I and II IR and relatively similar VCD. The type III minimizes to the type I and thus cannot be viewed as being a structure that one might easily discriminate experimentally with our spectral methods. It is clear that in COSMO, the two turns do minimize differently, but in the end their spectra are quite similar. The most critical distinguishing characteristic is the amide II VCD of the type II turn which is opposite in sign from the others. The other characteristic spectral variations relate to dispersion and small frequency shifts which would be very hard to identify in a multiconformational peptide or protein structure. Isotopic labeling might help in this regard by singling out the mode or allowing difference spectra to detect it [21,22,58–60,75,76].

One might have thought that solvation of C=O groups pointing out to solvent and in across the turn to form a H-bond would be quite different, leading to strong solvation effects. However, this was not true in our test cases, which admittedly were limited. The band shapes basically shifted with the diagonal terms and the local coupling and interactions stayed about the same. By extension, the diagonal terms shifted in a similar manner and did not have distinct local shifts we had expected. In general, the COSMO correction compressed the amide I modes to better reflect what is seen experimentally and may have dispersed the amide II. It is useful to realize that our preconception of which functional groups are H-bonded to water is overly structured as compared to the dynamic situation where the H-bonded interior residues are shielded and the outer ones are affected by side chains [60,61]. Such fixed water structure is chiral and has VCD contributions whereas the real dynamic situation is an average, essentially achiral, which reflects the correction being attempted by COSMO.

These turn patterns in IR and VCD are relatively weak in intensity and thus will not be the dominant features in the spectra of larger structures. To study the turns, one needs to isolate the unique bands. Isotope labeling offers some promise, but the mode must be carefully selected. Since the turns contribute to higher energy frequencies in the amide I, substituting $^{13}C=O$ will often just put those modes into overlap with the β-strand modes. Here, substitution with $^{13}C=^{18}O$ would be ideal [101,102].

The variations seen in this study give us a stronger understanding of where turn modes will contribute to the spectrum, evidence for their tendency to decouple from the rest of the peptide, and some idea of the VCD patterns one might see. Surprisingly, the key is not the strong amide I mode or its dipole coupling, but the weaker amide II which tends to give sign patterns discriminating between type I and II turns.

Acknowledgements This work was supported in part by a grant to TAK from the National Science Foundation (CHE03-16014) and by the Grant Agency of the Czech Republic (203/06/0420 to PB). Early studies were enabled by a Fellowship to TAK from the John Simon Guggenheim Memorial Foundation.

References

1. Mantsch HH, Chapman D (1996) Infrared spectroscopy of biomolecules. Wiley-Liss, Chichester
2. Barth A, Zscherp C (2002) Quart Rev Biophys 35:369
3. Haris PI (2000) In: Ram Singh B (eds) Infrared analysis of peptides and proteins: principles and applications. ACS Symposium Series. ACS, Washington DC, pp 54
4. Chi ZH, Chen XG, Holtz JSW, Asher SA (1998) Biochemistry 37:2854
5. Jordan T, Eads JC, Spiro TG (1995) Protein Sci 4:716
6. Keiderling TA, Silva RAGD (2002) In: Goodman M, Felix A, Moroder L, Toniolo C (eds) Synthesis of peptides and peptidomimetics. Georg Thieme Verlag, Stuttgart, pp 715
7. Keiderling TA (2002) Curr Opin Chem Biol 6:682
8. Keiderling TA (2000) In: Berova N, Nakanishi K, Woody RW (ed) Circular dichroism: principles and applications. Wiley, New York, pp 621
9. Nafie LA, Keiderling TA, Stephens PJ (1976) J Am Chem Soc 98:2715
10. Keiderling TA, Kubelka J, Hilario J (2005) In: Braiman M, Gregoriou V (ed) Vibratonal spectroscopy of polymers and biological systems. Marcel & Dekker, Amsterdam
11. Asher SA, Ianoul A, Mix G, Boyden MN, Karnoup A, Diem M, Schweitzer-Stenner R (2001) J Am Chem Soc 123:11775
12. Williams RW (1986) Methods Enzymol 130:311
13. Zhao XJ, Spiro TG (1998) J Raman Spectrosc 29:49
14. Barron LD, Hecht L, McColl IH, Blanch EW (2004) Mol Phys 102:731
15. Stephens PJ, Lowe MA (1985) Ann Rev Phys Chem 36:213
16. Stephens PJ (1987) J Phys Chem 91:1712
17. Devlin FJ, Stephens PJ, Cheeseman JR, Frisch MJ (1996) J Am Chem Soc 118:6327
18. Stephens PJ, Devlin FJ, Ashvar CS, Chabalowski CF, Frisch MJ (1994) Faraday Discuss 99:103
19. Cheeseman JR, Frisch MJ, Devlin FJ, Stephens PJ (1996) Chem Phys Lett 252:211
20. Bouř P, Kubelka J, Keiderling TA (2000) Biopolymers 53:380
21. Silva RAGD, Kubelka J, Decatur SM, Bouř P, Keiderling TA (2000) Proc Natl Acad Sci USA 97:8318
22. Huang R, Kubelka J, Barber-Armstrong W, Silva RAGD, Decatur SM, Keiderling TA (2004) J Am Chem Soc 126:2346
23. Fang C, Wang J, Charnley AK, Barber-Armstrong W, Smith AB III, Decatur SM, Hochstrasser RM (2003) Chem Phys Lett 382:586
24. Kubelka J, Huang R, Keiderling TA (2005) J Phys Chem B 109:8231
25. Krimm S, Bandekar J (1986) Adv Protein Chem 38:181
26. Frimand K, Bohr H, Jalkanen KJ, Suhai S (2000) Chem Phys 255:165
27. Choi JH, Kim JS, Cho M (2005) J Chem Phys 122:174903
28. Choi JH, Cho M (2004) J Chem Phys 120:4383

29. Toniolo C, Formaggio F, Tognon S, Broxterman QB, Kaptein B, Huang R, Setnicka V, Keiderling TA, McColl IH, Hecht L, Barron LD (2004) Biopolymers 75:32
30. Toniolo C, Benedetti E (1991) Trends Biol Sci 16:350
31. Kubelka J, Silva RAGD, Keiderling TA (2002) J Am Chem Soc 124:5225
32. Yoder G, Polese A, Silva RAGD, Formaggio F, Crisma M, Broxterman QB, Kamphuis J, Toniolo C, Keiderling TA (1997) J Am Chem Soc 119:10278
33. Yasui SC, Keiderling TA, Bonora GM, Toniolo C (1986) Biopolymers 25:79
34. Yasui SC, Keiderling TA, Formaggio F, Bonora GM, Toniolo C (1986) J Am Chem Soc 108:4988
35. Silva RAGD, Yasui SC, Kubelka J, Formaggio F, Crisma M, Toniolo C, Keiderling TA (2002) Biopolymers 65:229
36. Bouř P, Kubelka J, Keiderling TA (2002) Biopolymers 65:45
37. Elstner M, Jalkanen KJ, Knapp-Mohammady M, Frauenheim T, Suhai S (2000) Chem Phys 256:15
38. Han W, Elstner M, Jalkanen KJ, Frauenheim T, Suhai S (2000) Int J Quantum Chem 78:459
39. Dukor RK, Keiderling TA (1991) Biopolymers 31:1747
40. Keiderling TA, Xu Q (2002) Adv Protein Chem 62:111
41. Chellgren BW, Creamer TP (2004) Biochemistry 43:5864
42. McColl IH, Blanch EW, Hecht L, Kallenbach NR, Barron LD (2004) J Am Chem Soc 126:5076
43. Shi Z, Kallenbach NR, Woody RW (2002) Adv Protein Chem 62:163
44. Tiffany ML, Krimm S (1972) Biopolymers 11:2309
45. Tiffany ML, Krimm S (1968) Biopolymers 6:1379
46. Krimm S, Mark JE (1968) Proc Nat Acad Sci USA 60:1122
47. Bouř P, Keiderling TA (2004) J Mol Struct (THEOCHEM) 675:95
48. Kubelka J, Keiderling TA (2001) J Am Chem Soc 123:12048
49. Orengo CA, Jones DT, Thornton JM (1994) Nature 372:631
50. Wilmot CM, Thornton JM (1988) J Mol Biol 203:221
51. Rose GD, Gierasch LM, Smith JA (1985) Adv Protein Chem 37:1
52. Hollosi M, Majer ZS, Ronai AZ, Magyar A, Medzihradszy K, Holly S, Perczel A, Fasman GD (1994) Biopolymers 34:177
53. Vass E, Hollosi M, Besson F, Buchet R (2003) Chem Rev 103:1917
54. Toniolo C (1980) CRC Crit Rev Biochem 9:1
55. Xie P, Zhou Q, Diem M (1994) Faraday Discuss 99:233
56. Polavarapu PL, Deng ZY (1996) Faraday Discuss 99:151
57. Kubelka J, Silva RAGD, Bouř P, Decatur SM, Keiderling TA (2002) In: Hicks JM (ed) Chirality: physical chemistry. ACS Symposium Series. American Chemical Society, Washington, pp 50
58. Kubelka J, Keiderling TA (2001) J Am Chem Soc 123:6142
59. Bouř P, Keiderling TA (2005) J Phys Chem B 109:5348
60. Bouř P, Keiderling TA (2005) J Phys Chem B 109:23687
61. Kim J, Huang R, Kubelka J, Bouř P, Keiderling TA (2006) J Phys Chem B (in press)
62. Bouř P, Sopková J, Bednárová L, Maloň P, Keiderling TA (1997) J Comput Chem 18:646
63. Hilario J, Kubelka J, Keiderling TA (2003) J Am Chem Soc 125:7562
64. Ragothama SR, Awasthi SK, Balaram P (1998) J Chem Soc Perkin Trans 2:137
65. Eker F, Cao X, Nafie L, Schweitzer-Stenner R (2002) J Am Chem Soc 124:14330
66. Jalkanen KJ, Jurgensen VW, Claussen A, Rahim A, Jensen GM, Wade RC, Jung C, Degtyarenko IM, Nieminen RM, Herrmann F, Knapp-Mohammady M, Niehaus TA, Frimand K, Suhai S (2006) Int J Quantum Chem 106:1160
67. Kim YS, Wang J, Hochstrasser RM (2005) J Phys Chem B 109:7511
68. Woutersen S, Hamm P (2000) J Phys Chem B 104:11316
69. Kubelka J, Kim J, Bouř P, Keiderling TA (2006) Vib Spectrosc (in press)
70. Kubelka J, Keiderling TA (2001) J Phys Chem A 105:10922
71. Bouř P, Keiderling TA (2003) J Chem Phys 119:11253
72. Cho M (2003) J Chem Phys 118:3480
73. Besley NA (2004) J Phys Chem A 108:10794
74. Kwac K, Cho M (2003) J Chem Phys 119:2247
75. Setnicka V, Huang R, Thomas CL, Etienne MA, Kubelka J, Hammer RP, Keiderling TA (2005) J Am Chem Soc 127:4992
76. Huang R, Setnicka V, Thomas CL, Etienne MA, Kubelka J, Kim J, Hammer RP, Keiderling TA (2006) (to be submitted)
77. Baello BI, Pancoska P, Keiderling TA (1997) Anal Biochem 250:212
78. Singh BR, Fu FN, Ledoux DN (1994) Nature Struct Biol 1:358
79. Griebenow K, Klibanov AM (1995) Proc Nat Acad Sci USA 92:10969
80. Thomas CL, Etienne MA, Wang J, Setnicka V, Keiderling TA, Hammer RP (2003) Peptide revolution: genomics proteomics, and therapeutics. In: Proceedings of the 18th American peptide society meeting, San Diego, 2004
81. Stanger HE, Syud FA, Espinosa JF, Giriat I, Muir T, Gellman SH (2001) Proc Natl Acad Sci USA 98:12015
82. Kubelka J (2002) Ph.D. thesis, University of Illinois at Chicago.
83. Frisch MJ, Trucks GW, Schlegel HB, Scuseria GE, Robb MA, Cheeseman JR, Montgomery JA, Vreven JT, Kudin KN, Burant JC, Millam JM, Iyengar SS, Tomasi J, Barone V, Mennucci B, Cossi M, Scalmani G, Rega N, Petersson GA, Nakatsuji H, Hada M, Ehara M, Toyota K, Fukuda R, Hasegawa J, Ishida M, Nakajima T, Honda Y, Kitao O, Nakai H, Klene M, Li X, Knox JE, Hratchian HP, Cross JB, Adamo C, Jaramillo J, Gomperts R, Stratmann RE, Yazyev O, Austin AJ, Cammi R, Pomelli C, Ochterski JW, Ayala PY, Morokuma K, Voth GA, Salvador P, Dannenberg JJ, Zakrzewski VG, Dapprich S, Daniels AD, Strain MC, Farkas O, Malick DK, Rabuck AD, Raghavachari K, Foresman JB, Ortiz JV, Cui Q, Baboul AG, Clifford S, Cioslowski J, Stefanov BB, Liu G, Liashenko A, Piskorz P, Komaromi I, Martin RL, Fox DJ, Keith T, Al-Laham MA, Peng CY, Nanayakkara A, Challacombe M, Gill PMW, Johnson B, Chen W, Wong MW, Gonzalez C, Pople JA, Gaussian 03. Gaussian Inc., Pittsburgh, PA, 2003
84. Klamt A (1998) In: Schleyer PR, Allinger NL, Clark T, Gasteiger J, Kollman PA, Schaefer HF III, Schreiner PR (eds) The encyclopedia of computational chemistry. Wiley, Chichester, pp 604
85. Tomasi J, Persico M (1994) Chem Rev 94:2027
86. Bouř P (2004) J Chem Phys 121:7545
87. Han W, Jalkanen KJ, Elstner M, Suhai S (1998) J Phys Chem B 102:2587
88. Polavarapu PL, Zhao C, Das C, Balaram P (2000) J Am Chem Soc 122:8228
89. Du D, Zhu Y, Huang C, Gai F (2004) Proc Natl Acad Sci USA 101:15915
90. Yang W-Y, Pitera JW, Swope WC, Gruebele M (2004) J Mol Biol 336:241
91. Stanger HE, Gellman SH (1998) J Am Chem Soc 120:4236
92. Gellman SH (1998) Curr Opin Struct Biol 2:717
93. Fu F, DeOliveira DB, Trumble WR, Sarkar HK, Singh BR (1994) Appl Spectrosc 48:1432

94. Cai S, Singh BR (2000) In: Singh BR (ed) Infrared analysis of peptides and proteins: principles and applications. ACS Symposium Series. ACS, Washington, pp 117
95. Cheeseman JR, Frisch MJ, Devlin FJ, Stephens PJ (2000) J Phys Chem 104:1039
96. Stephens PJ, Devlin FJ (2000) Chirality 12:172
97. Torii H, Tatsumi T, Tasumi M (1998) J Raman Spec 29: 537
98. Brauner JW, Dugan C, Mendelsohn R (2000) J Am Chem Soc 122:677
99. Brauner JW, Flack CR, Mendelsohn R (2005) J Am Chem Soc 127:100
100. Paul P, Axelsen PH (2005) J Am Chem Soc 127:5754
101. Arbely E, Kass I, Arkin IT (2003) Biophys J 85:2476
102. Torres J, Kukol A, Goodman JM, Arkin IT (2001) Biopolymers 59:396